

Compact-sized and broadband carpet cloak and free-space cloak

Hui Feng Ma, Wei Xiang Jiang, Xin Mi Yang, Xiao Yang Zhou, and Tie Jun Cui*

State Key Laboratory of Millimeter Waves and Institute of Target Characteristics and Identification

Department of Radio Engineering, Southeast University, Nanjing 210096, P. R. China.

Abstract

Recently, invisible cloaks have attracted much attention due to their exciting property of invisibility, which are based on a solid theory of transformation optics and quasi-conformal mapping. Two kinds of cloaks have been proposed: free-space cloaks, which can render objects in free space invisible to incident radiation, and carpet cloaks (or ground cloaks), which can hide objects under the conducting ground. The first free-space and carpet cloaks were realized in the microwave frequencies using metamaterials. The free-space cloak was composed of resonant metamaterials, and hence had restriction of narrow bandwidth and high loss; the carpet cloak was made of non-resonant metamaterials, which have broad bandwidth and low loss. However, the carpet cloak has a severe restriction of large size compared to the cloaked object. The above restrictions become the bottlenecks to the real applications of free-space and carpet cloaks. Here we report the first experimental demonstration of broadband and low-loss directive free-space cloak and compact-sized carpet cloak based on a recent theoretical study. Both cloaks are realized using non-resonant metamaterials in the microwave frequency, and good invisibility properties have been observed in experiments. This approach represents a major step towards the real applications of invisibility cloaks.

PACS numbers. 41.20.Jb, 42.25.Gy, 42.79.-e

*tjcui@seu.edu.cn

Recently, a new theory of transformation optics and quasiconformal mapping has been proposed to design the electromagnetic metamaterials to control the paths of electromagnetic waves [1,2,4]. Based on the physical principle, an electromagnetic wave will always travel in the quickest route between two points. In a homogeneous and isotropic material, the route is a straight line. In an inhomogeneous material, the route becomes nonlinear to make the total traveling time be minimal because the wave travels at different speeds inside. Hence one can control the route of wave by designing the material parameters, which has found a lot of potential applications such as cloaking objects invisible [1-7], concentrating of electromagnetic waves [8,9], rotating of electromagnetic waves [10], bending of electromagnetic waves [11], and forming multi-beam antennas [12]. Artificial metamaterials provide flexible choices of the designed parameters.

Among above potential applications, the invisibility cloak is the most attractive. There have been two kinds of invisibility cloaks proposed: free-space cloaks and carpet cloaks. A free-space cloak is a designed material shell covering an object in free space, which can guide the waves to propagate around the shell, making the object inside invisible [1]. The theoretical tool to study invisible cloak is the so-called transformation optics [13], which is based on the coordinate transformation [14]. An optical conformal mapping method was used to design the material parameters that create perfect invisibility [1,2], in which the permittivity tensor ϵ and the permeability tensor μ are both spatially varying and anisotropic with singular values. By implementing such complicated full material properties, the concealed object and the cloak appear to have the free-space properties exactly when viewed externally, which has been verified by full-wave simulations [15] and analytic solutions [16].

However, the fully inhomogeneous and anisotropic parameters for perfect free-space cloaks require extremely complicated metamaterial design. For a two-dimensional (2D) cylindrical cloak in free space, when the electric field is polarized along the cylinder axis, the full parameters can be greatly simplified [3]. Since the reduced constitutive parameters provide the same dispersion equation as the full parameters for the 2D cloak, the electromagnetic waves have the same trajectory inside the cloak with a penalty of nonzero reflections. Using the reduced parameters, the first practical free-space cloak has been realized in the microwave frequency [3]. In the experiment, a conducting cylinder was hidden inside the cloak, which was constructed with the use of artificially structured metamaterials. Due to the requirement of very large and very small values of refraction index, resonant structures [17] have been applied. This makes the invisible cloak operate in a narrow frequency band with a relatively large loss. The experiment and simulation results have a good match. But notable reflections and shadow of the hidden object were observed due to the use of simplified parameters and relatively large loss [3]. The narrow bandwidth and large loss become the big restriction to

real applications of free-space cloaks.

In view of the difficulty to realize the free-space cloaks, a recently published theory has suggested a carpet cloak, or ground-plane cloak, which can hide any objects under a metamaterial carpet [4]. Different from the free-space invisibility cloak, which crushes the cloaked object to a point, the carpet cloak crushes the hidden object to a conducting sheet [4]. In the other word, any objects hidden under the carpet appear as a flat conducting sheet, and hence cannot be detected by any exterior sources. The great advantage of the carpet cloak is that it does not require singular values for the material parameters [1]. By choosing appropriate coordinate transformation, it has been shown that the anisotropy of the cloak can be minimized and the range of the permittivity and permeability is much smaller than that for the free-space cloak [4]. Hence the carpet cloak is easier to be realized using metamaterials.

The carpet cloak has very important applications, especially in the microwave frequencies. For example, it can be used to hide the aircraft on the airport, and the automobile on the ground, etc. The carpet cloaks have been experimentally demonstrated firstly in the microwave frequency [5], and then in the optical frequency [6,18], using non-resonant metamaterials. The non-resonant metamaterials have very low loss and operate in a broad frequency band, hence the carpet cloaks have good invisibility performance [5,6]. However, there are two restrictions in the existing carpet-cloak experiments: 1) the background is not free space to get easily realized material parameters (in the microwave experiment, the refractive index of background material was chosen as 1.331 [5]; in the optical experiment, the refractive index of background material was chosen as 1.58 [6]); 2) the carpet cloak has a very large size (in the microwave experiment, the area ratio of the carpet cloak to the cloaked region is as high as 65.7 [5]). The above restrictions make the carpet cloak be difficult in real applications.

Here, we demonstrate experimentally the first broadband and low-loss directive free-space cloak and compact-sized carpet cloak in the free-space background. The experiments are based on a recent theoretical study [7], which proposed a simplified carpet cloak (or ground-plane cloak) made of only a few blocks of all-dielectric isotropic materials. In our experiments, the simplified carpet cloak is realized using non-resonant metamaterials in the microwave frequency, which has a much smaller size than the full carpet cloak reported in Ref. [5]. The area ratio of the cloak to the cloaked region is as small as 7.33, which is only 11.2% of the full cloak. However, the presented carpet cloak has equally good invisibility performance. Furthermore, a broadband and low-loss directive free-space cloak is realized, that cloaks the radiation originating from specified directions. Hence the presented work makes a major step towards the real applications of invisibility cloaks.

For the design of the simplified carpet cloak, we consider a 2D problem in which all the fields are invariant in the z direction and the electric fields are z -polarized. The cloaked object is a car model, which is placed under a triangular conducting region. The reason to choose the triangular shape is for easy installation in real applications. We want to design a compact-sized carpet cloak which is covering on the triangular region to make the whole system appear as the original flat conducting plane as if the car does not exist. We choose the shape of cloak as a rectangle with the width 125 mm and height 50 mm except that the bottom boundary is partially triangularly-shaped to place the car. Hence the car model is concealed between the carpet cloak and the conducting plane as shown in Fig. 1(c).

To design a compact-sized carpet cloak, the process of parameter calculation contains two stages. First, we followed the technique presented in [4] to get the complete cloaking region, in which a quasi-conformal coordinate mapping is generated by minimizing the Modified-Liao functional [20, 21] upon slipping boundary condition. The refractive-index distribution of the cloak is computed numerically, as shown in Fig. 1(a), in which the maximum anisotropic factor is 1.07. Secondly, we use the grid optimization by recursive division of Cartesian cells to sample the original refractive-index distribution. In such a course, the small regions near the base corners of the triangular object where the refractive-index is smaller than 1 are treated as free space. Since the background of the designed cloak is free space, the transformation generates cells in region I (Fig. 1(a)) whose refractive indices are nearly 1. Hence such a region can be simplified as free space, and the cloak will reduce to the region II (Fig. 1(a)). The refractive index distribution of the final carpet cloak is illustrated in Fig. 1(b), in which the refractive indices are varied from 1 to 1.69.

The compact-sized carpet cloak is divided to 3-by-3-mm squares with non-resonant elements shown in Figs. 1(c) and 1(d). By changing the dimension h (see Fig. 1(d)) from 0 to 2.2 mm, we are able to span the required index range from $n = 1.07$ to 1.87 at 10 GHz. After a well-established retrieval process, the effective permittivity and permeability for a given element can be found by numerical simulation. Fig. 1(d) shows the curve that relates the refractive index to a given element with the length h . Since the cell-to-cell change in dimension is minor, the impedance is matched gradually in the whole cloak over the entire measurement frequency range. The compact-sized carpet cloak is fabricated on copper-clad printed circuit board (PCB) with F4B substrate (the substrate thickness is 0.25 mm, with a dielectric constant of 2.65 and loss tangent of 0.001). The carpet has a size of $125 \times 50 \text{ mm}^2$ with a height of 12 mm. The cloaking transformation is specifically designed to compensate the triangular concealed region with the height 13 mm and the bottom 125 mm.

To validate the invisible effect of the simplified carpet cloak, we make use of a near-field scanning

system to map the electric-field distribution within a planar waveguide. In the planar waveguide, the wave polarization is restricted to transverse electric. The electric-field maps of the scattering region, including the collimated incident and scattered beams, are shown in Fig. 2. The incident waves are launched into the chamber from a standard X-band coax-to-waveguide coupler to produce a nearly collimated microwave plane beam. The beam is arbitrarily chosen to be incident on the ground plane at an angle of 45° with respect to the normal.

Figure 2 shows the measured near-field distributions and the far-field patterns of the carpet cloak. From Figs. 2(a) and (b), there is considerable difference between the reflections from the flat and curved surfaces. The beam reflected from the uncloaked triangular bump shows the strong scattering of the bump. The flat surface illustrates the expected collimation beam profile, similar to that of the incident wave. To hide the bump on the surface, the designed carpet cloak was placed around the bump and the measured result is shown in Fig. 2(c). Subsequently, similar to the flat reflecting surface, a single reflected beam is observed. This demonstrates that the cloak has successfully transformed the curved surface into a flat surface, giving the observer the impression that the beam was reflected from a flat surface. Owing to the fact that there is no penetration of light into the bump, the car model could be placed behind it and effectively hidden, making the car invisible. The far-field patterns are plotted in Figs. 2(g)-(i). For the ground plane and the cloaked triangular concealed region, the beam profiles show a very similar single peak; that is, the good cloaking performance is observed. Unlike the above cases, the bump alone exhibits a multi-peak far-field pattern (Fig. 2h), indicating the strong perturbation of the beam.

To verify the broadband properties of the carpet cloak, measurements were carried out over a wide range of frequencies. The cloaking behavior was confirmed in our measurements from 10 GHz to 13 GHz, as shown in Figs. 2(d), (e) and (f). The cloak is expected to work very well within a more wide frequency band although it cannot be verified experimentally due to limitations of the measurement apparatus. Figs. 2(d)-2(f) show similar cloaking behavior to the map taken at 10 GHz in Fig. 2(c).

The compact-sized carpet cloaks discussed above only work in the presence of ground-plane. Next, we consider a compact-sized and broadband free-space cloak based on the electromagnetic mirror principle although the free-space cloak works only for a specified direction, as suggested in [4, 7]. Such a kind of directive free-space cloaks can also find a lot of specific applications like air flight, space exploration, etc. For practical reason, here we choose the outer boundary of the free-space cloak as a prolate cylinder, whose long axis is 125 mm and short axis is 60 mm (see Fig. 3). Starting from the compact-sized carpet cloak design shown in Fig. 3(a), which is similar to Fig. 1(a), the ground plane is removed and the cloaked

region in company with the object is mirrored on $y = 0$. As a result, a metallic diamond-shaped object is surrounded with a free-space compact-sized cloaking material, as shown in Fig 3(b). Figs. 3(c) and 3(d) illustrate the photos of the free-space cloak and the diamond-shaped conducting object in free-space background. In the experiment, a foam, whose electromagnetic properties are similar to free space, was used to fix the metamaterials. Since the refractive indices on two sides of the cloak along the x axis are almost one as marked by the red dashed lines in Fig. 3(b), such areas can be designed as free space. The sample is fabricated by using non-resonant metamaterial unit elements similar to the compact-sized carpet cloak presented earlier.

To visualize the performance of the compact-sized and broadband free-space cloak, we make full-wave simulations based on the finite-element method. In principle, an incident electromagnetic wave would perceive a perfectly cloaked object as a metallic surface in the $y = 0$ plane with infinitesimal thickness. Such a device will scatter the impinging wave significantly for most incident angles, except when the wave is propagating along the x direction. The simulation results are illustrated in Figs. 4(a) and (b) when a plane wave is impinging upon a conducting diamond-shaped object without and with the free-space cloak. A very strong shadow is observed behind the bare object, along with a weak backward scattering pattern due to the sharp edge of the diamond object (Fig. 4(a)). Subsequently, the designed cloak is placed around the diamond object. We observe that there is no shadow left as the wavefronts are bending and recomposing on the back of the object, with only a slight distortion, as shown in Fig. 4(b). Hence, the object would be effectively cloaked.

The measurement results of the diamond-shaped metallic object without and with the free-space directive cloak are shown in Figs. 4(c) and 4(d) when the collimated beam is incident horizontally at 10 GHz. Obviously, the measured field patterns have excellent agreements to the simulation results. From Fig. 4(d), we observe that when the wave reaches the left corner of the diamond-shaped metallic object, the index gradient is increasing away from the boundary of the object, and hence the wave bends away from the object. Then, near the tip of the object, the wave bends back towards the object because the index gradient is reversed. Finally, due to the increasing index gradient away from the object near the right corner, the wave is bent away from the object, and then return back to their original propagation direction.

To verify the broadband properties of the free-space cloak, measurements were implemented over a wide range of frequencies. The cloaking behavior has been confirmed in these measurements from 8 to 12 GHz. We illustrate the broad bandwidth of the cloak with the field maps taken at 8 GHz in Fig. 4(e), 9 GHz in Fig. 4(f), 11 GHz in Fig. 4(g) and 12 GHz in Fig. 4(h), which show similar cloaking behavior to

the map taken at 10 GHz in Fig. 4(d). This method would be increasingly favorable for compact-sized cloaking objects in free-space background when considering its design simplicity, since only a few blocks of all-dielectric materials are required in order to achieve broadband and low-loss performance.

Both compact-sized carpet cloak and directive free-space cloak are designed based on the isotropic and non-resonant unit elements, hence the presented cloaks are broadband and low-loss. The agreement between the measured field patterns and the theory [7] provides convincing evidence that metamaterials can indeed be widely applied in practice. The experimental demonstration of compact-sized invisibility cloaks represents a major step towards real applications of invisibility devices.

This work was supported in part by the National Science Foundation of China under Grant Nos. 60990320, 60990324, 60671015, 60871016, and 60901011, in part by the National Basic Research Program (973) of China under Grant No. 2004CB719802, in part by the Natural Science Foundation of Jiangsu Province under Grant No. BK2008031, and in part by the 111 Project under Grant No. 111-2-05.

References

- [1] J. B. Pendry, D. Schurig and D. R. Smith, *Science* **312**, 1780-1782 (2006).
- [2] U. Leonhardt, *Science* **312**, 1777-1780 (2006).
- [3] D. Schurig, J. J. Mock, B. J. Justice, S. A. Cummer, J. B. Pendry, A. F. Starr and D. R. Smith, *Science* **314**, 977-980 (2006).
- [4] J. Li and J. B. Pendry, *Phys. Rev. Lett.* **101**, 203901 (2008).
- [5] R. Liu, C. Ji, J. J. Mock, J. Y. Chin, T. J. Cui and D. R. Smith, *Science* **323**, 366-369 (2009).
- [6] J. Valentine, J. Li, T. Zentgraf, G. Bartal and X. Zhang, *Nature Mater.* **8**, 568-571 (2009).
- [7] E. Kallos, C. Argyropoulos and Y. Hao, *Phys. Rev. A* **79**, 063825 (2009).
- [8] M. Rahm, D. Schurig, D. A. Roberts, S. A. Cummer, D. R. Smith and J. B. Pendry, *Phot. Nano.-Fund. Appl.* **6**, 87-95 (2008).
- [9] W. X. Jiang, T. J. Cui, Q. Cheng, J. Y. Chin, X. M. Yang, R. Liu and D. R. Smith, *Appl. Phys. Lett.* **92**, 264101 (2008).
- [10] H. Chen and C. T. Chan, *Appl. Phys. Lett.* **90**, 241105 (2007).
- [11] W. X. Jiang, T. J. Cui, X. Y. Zhou, X. M. Yang and Q. Cheng, *Phys. Rev. E* **78**, 066607 (2008).
- [12] W. X. Jiang, T. J. Cui, H. F. Ma, X. Y. Zhou and Q. Cheng, *Appl. Phys. Lett.* **92**, 261903 (2008).
- [13] D. Schurig, J. B. Pendry and D. R. Smith, *Opt. Express* **14**, 9794-9804 (2006).
- [14] U. Leonhardt and T. G. Philbin, *New J. Phys.* **8**, 247 (2006).
- [15] S. A. Cummer, B.-I. Popa, D. Schurig and D. R. Smith, *Phys. Rev. E* **74**, 036621 (2006).
- [16] H. Chen, B.-I. Wu, B. Zhang and J. A. Kong, *Phys. Rev. Lett.* **99**, 063903 (2007).
- [17] J. B. Pendry, A. J. Holden, D. J. Roberts and W. J. Stewart, *IEEE Trans. Micro. Theory Tech.* **47**, 2075-2084 (1999).
- [18] L. H. Gabrielli, J. Cardenas, C. B. Poitras and M. Lipson, *Nat. Photon.* **3**, 461-463 (2009).
- [19] A. Greenleaf, Y. Kurylev, M. Lassas and G. Uhlmann, *Phys. Rev. Lett.* **99**, 183901 (2007).

- [20] P. Knupp and S. Steinberg, Fundamentals of Grid Generation (CRC Press, Boca Raton, 1994).
- [21] J. F. Thompson, B. K. Soni and N. P. Weatherill, Handbook of Grid Generation (CRC Press, Boca Raton, 1999).

List of Figure Captions

Fig. 1: The design for a compact-sized carpet cloak in free-space background. (a) Metamaterial refractive index distribution of the complete carpet cloaking region in which the mesh lines indicate the quasi-conformal mapping. The compact-sized cloaking region is shown within the box. (b) Expanded view of the compact-sized cloaking region in which the refractive indices below one are all designed as 1. (c) Photograph of the fabricated metamaterial carpet cloak and the concealed car model. (d) The design of non-resonant elements and the relation between the unit cell geometry and the effective index. The dimensions of the metamaterial unit cells are $a = 3$ mm, $w = 0.2$ mm, $l = h + 2w$ mm, and h varying from 0 to 2.2 mm.

Fig. 2: (color online) Measured electric-field mapping of (a) the ground plane, (b) triangular metallic bump, and (c) ground-plane cloaked bump when collimated beam is incident at 10GHz. The rays display the wave propagation direction, and the dashed line indicates the normal of the ground in free space and that of the ground-plane cloak in the transformed space. (d) Collimated beam incident on the ground-plane cloaked bump at 11 GHz. (e) Collimated beam incident on the ground-plane cloaked bump at 12 GHz. (f) Collimated beam incident on the ground-plane cloaked bump at 13 GHz. Far-field patterns when collimated beam is incident at 10 GHz on (g) the ground plane, (h) the triangular metallic bump, (i) the carpet cloaked bump.

Fig. 3: (color online) The transformation optical design for the directive free-space cloak. The metamaterial cloak region is embedded in free-space background. (a) Refractive index distribution of half free-space cloak in which the mesh lines indicate the quasi-conformal mapping. (b) Expanded view of the free-space cloaking region in which the refractive indices below one are all designed as 1. (c) The photo of the fabricated metamaterial sample. (d) The side elevation of the fabricated metamaterial sample.

Fig. 4: (color online) Simulated electric-field distribution of the directive free-space cloak when a plane wave is incident at 10 GHz on (a) the bare metallic diamond-shaped object, (b) on the cloaked diamond-shaped object at 10 GHz. The rays display the wave propagation direction. Measured electric-field mapping of the directive free-space cloak when a plane wave is incident on (c) the bare metallic diamond-shaped object at 10 GHz, (d) the cloaked diamond-shaped object at 10 GHz, (e) the cloaked diamond-shaped object at 8 GHz, (f) the cloaked diamond-shaped object at 9 GHz, (g) the cloaked diamond-shaped object at 11 GHz, (h) the cloaked diamond-shaped object at 12 GHz.

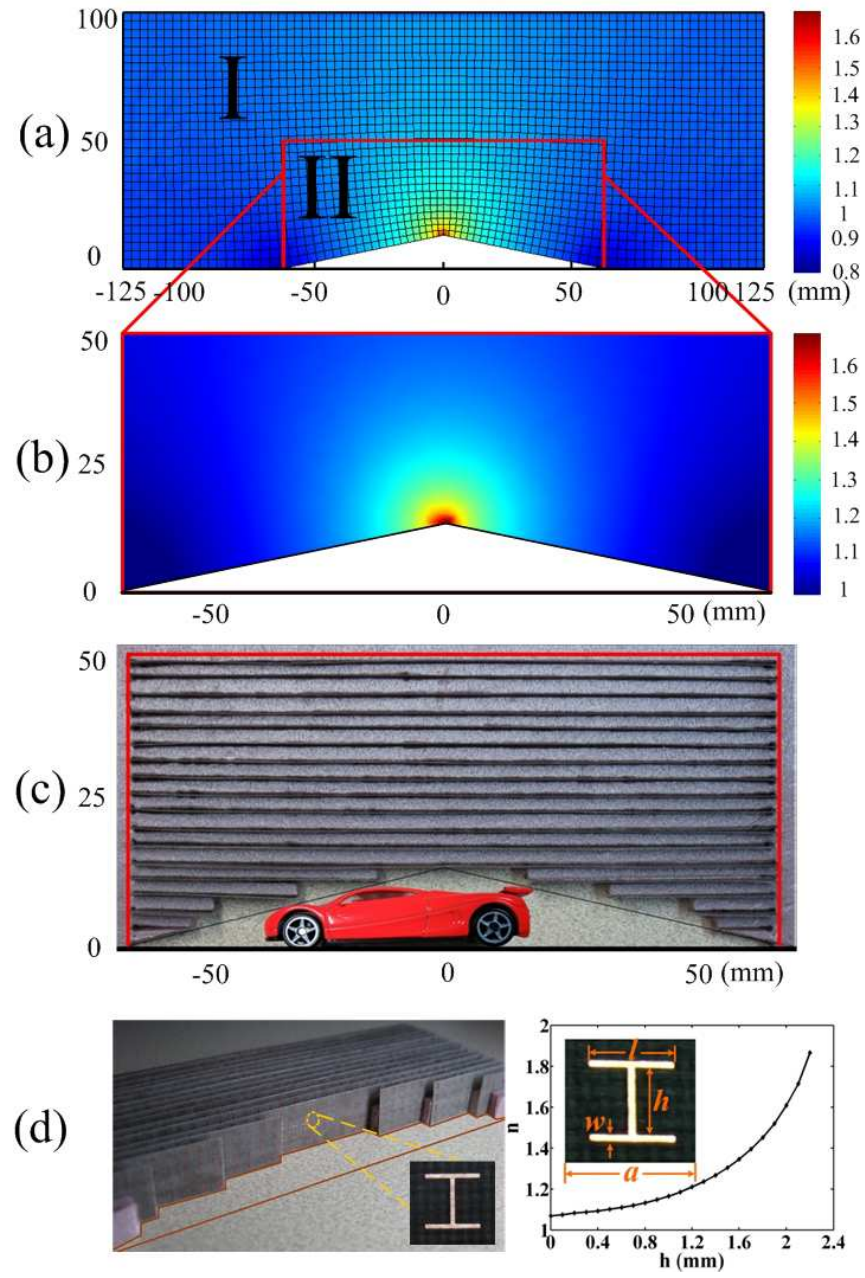


Figure 1:

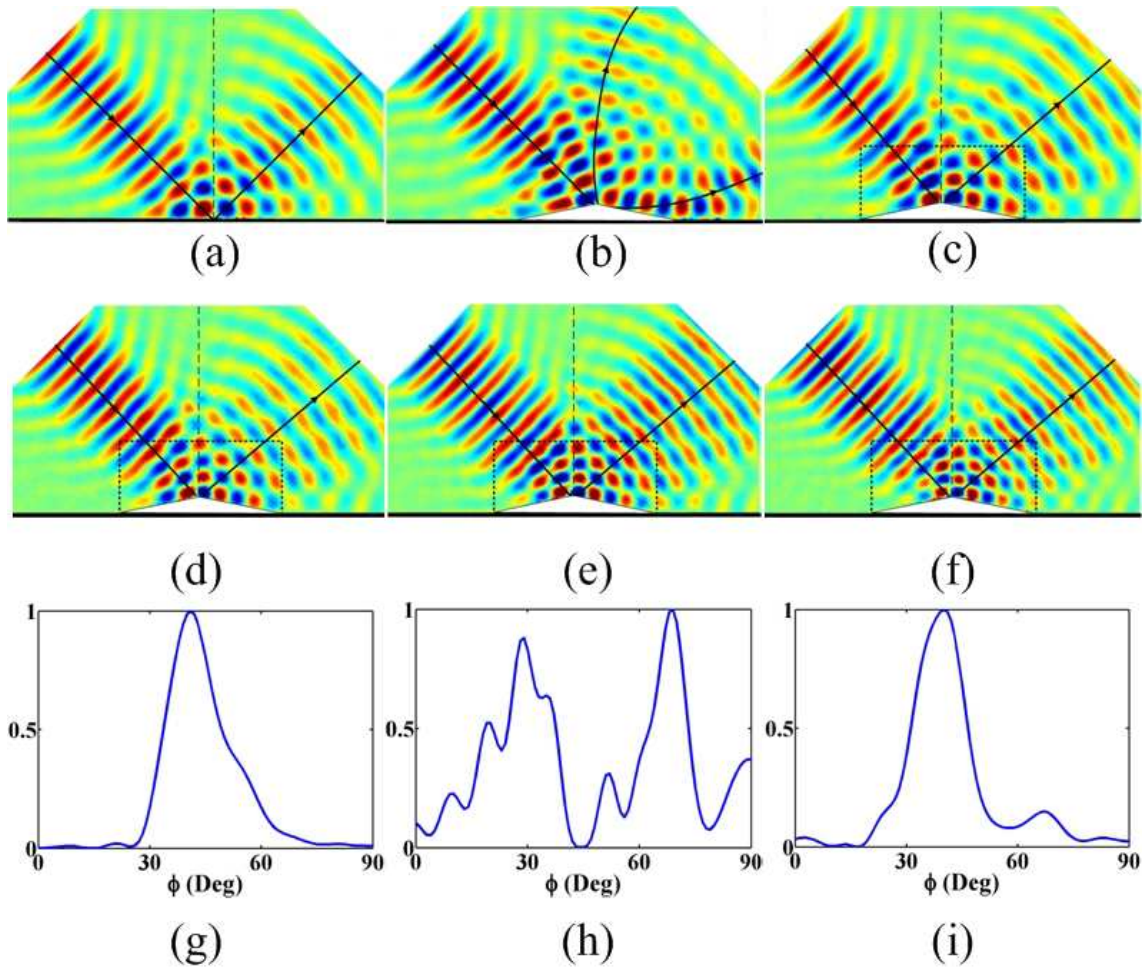


Figure 2:

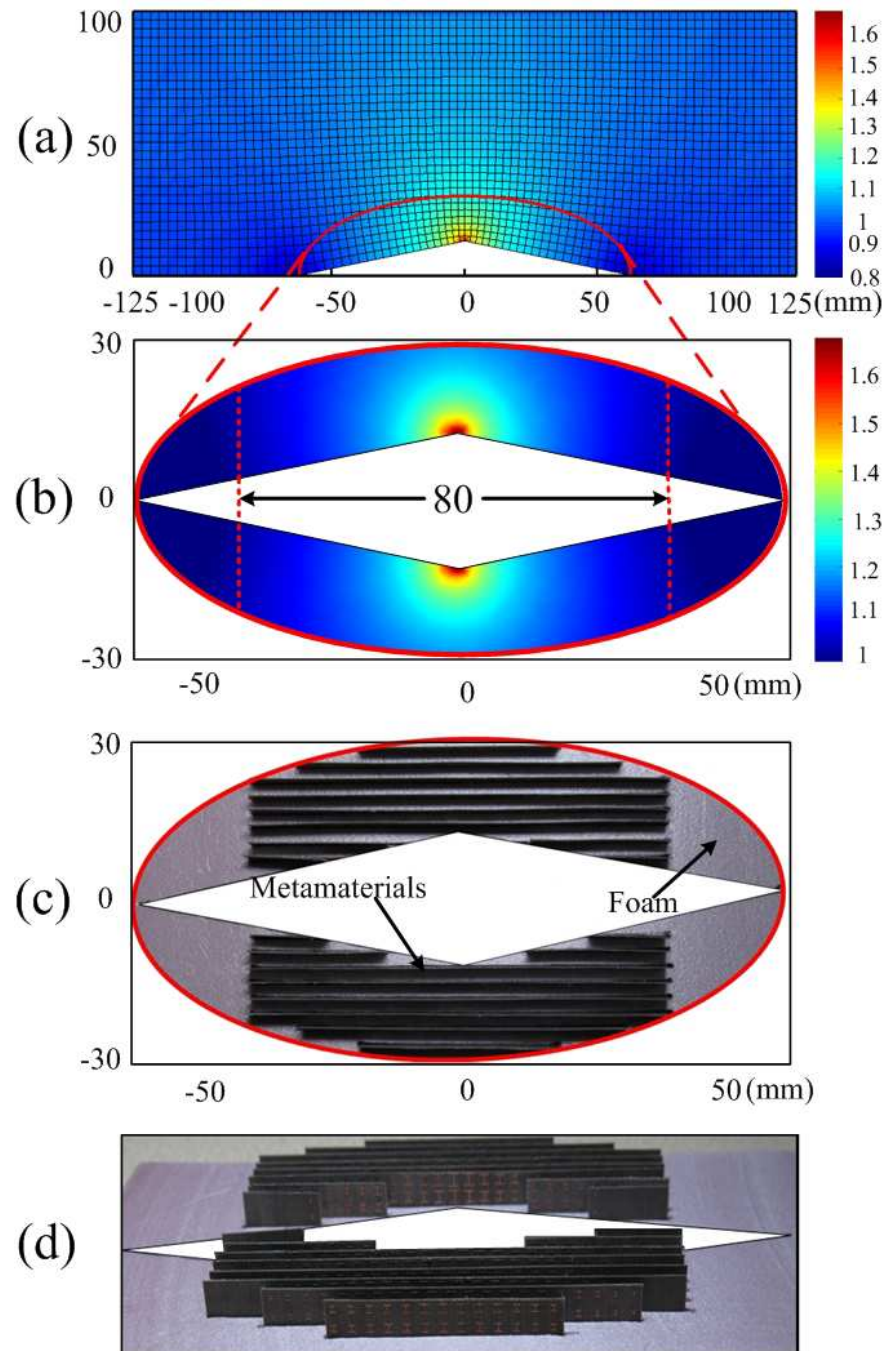


Figure 3:

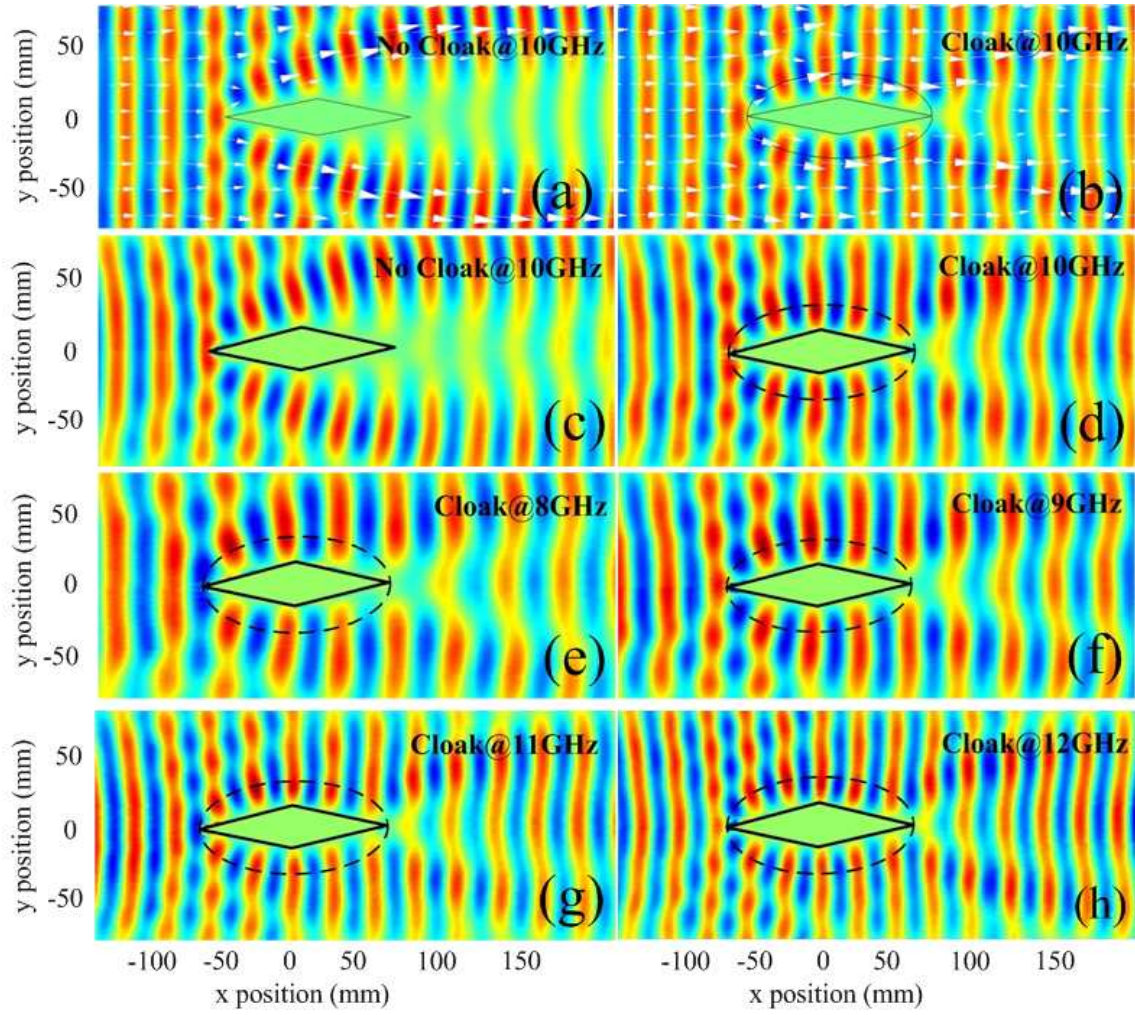


Figure 4: